Journal of Advanced College of Engineering and Management

Comparative Focal Mechanism and Fault Plane Ambiguity Analysis of the 2015 Gorkha Earthquake Using Global CMT and DMG Catalogs

[1*]Gaurav Panth, [2]Prajesh Gyawali, [3]Binaya Prasad Dhakal, [4]Ishwor Panta
[1,3,4]*Department of Civil Engineering, Advanced College of Engineering and Management*
[2]*Department of Civil Engineering, Thapathali Campus*
Corresponding email: [*]gaurav.panth@acem.edu.np

DOI: 10.3126/jacem.v12i01.93940

Abstract

On April 25, 2015, Nepal was struck by an Mw 7.8 earthquake. This study characterizes the source mechanism using focal mechanism solutions (beach balls) derived from the Global Centroid Moment Tensor (CMT) and Department of Mines and Geology (DMG) catalogs. The results confirm a thrust-faulting mechanism with strike, dip, and rake angles consistent with the regional tectonic framework. The rupture initiated near the hypocenter and propagated southeastward along the dip direction, a trajectory supported by finite-fault modeling. As no shallow surface rupture was observed, this rupture direction is supported by aftershock distribution, stereonet P-axis orientation, and finite-fault modeling studies. These findings improve understanding of rupture geometry and help identify potential seismic hazard zones in central Nepal.

Keywords—*Gorkha Earthquake, Focal Mechanism, Thrust Fault, Moment Tensor*

1. INTRODUCTION

A. Background

The 2015 Gorkha earthquake was caused by thrust faulting on or near the primary contact between the subducting India plate and the overriding Eurasia plate. While the rupture process has been studied, a clear gap exists in localized comparative analysis between the DMG and Global CMT catalogs using GIS-based visualization. The objective of this study is to bridge this gap by mathematically characterizing the source mechanism and validating the nodal plane orientation to better understand the seismic hazard in Central Nepal. Despite several studies on the 2015 Gorkha earthquake, a systematic comparison of focal mechanism solutions derived from both Global CMT and DMG catalogs using GIS-based visualization and stereonet validation remains limited. This study aims to fill this gap.

B. Objectives

(1) Compute and compare beachball focal mechanisms from both catalogs;

(2) Use stereonet and moment tensors to quantify thrust fault geometry

(strike/dip/rake);

(3) Analyze aftershock patterns to identify locked segments needing monitoring

C. Geo-tectonics of the region

The four tectonic groups are separated by the Main Frontal Thrust (MFT), Main Boundary Thrust (MBT), Main Central Thrust (MCT), and South Tibet Detachment (STD) (Figure 1). The active thrust fault known as the MFT is located near the southern boundary of the Sub-Himalayan foothills. [1]

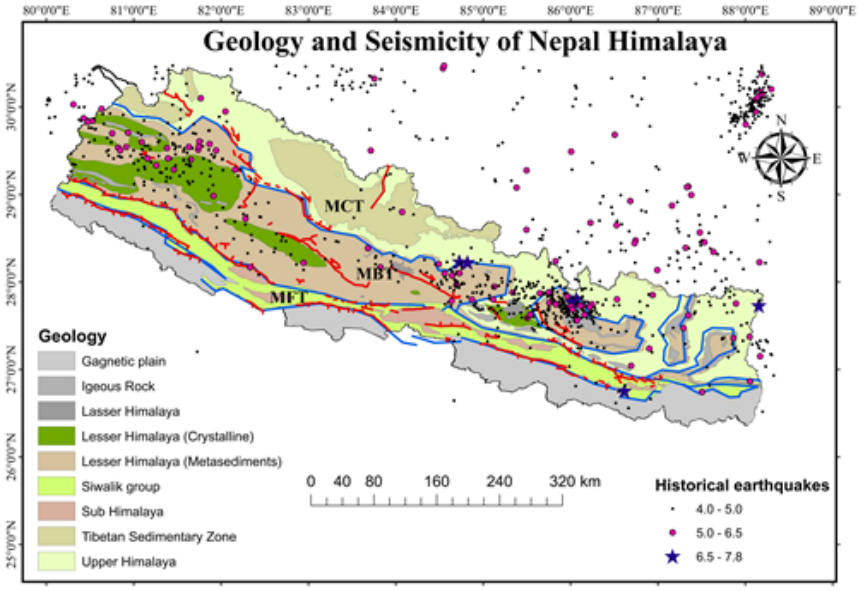

Figure 1: Active Faults of Nepal (Source: [1])

D. Fault Plane Solution

The orientation of an earthquake fault can be inferred from seismic records obtained at stations distributed around the source. This approach, known as a fault plane solution, relies primarily on the polarity of the first arriving P-waves. Because the radiation of seismic energy depends on how the fault slips, the initial motion recorded at each station carries information about the geometry of the rupture [2].

As P-waves travel outward from the hypocenter, the first ground motion detected at a station is either compressional or dilatational. A compressional arrival indicates that ground particles moved toward the station at the onset of the wave, whereas a dilatational arrival indicates motion away from the station. When these observations are plotted around the source, they divide the surrounding space into four sectors: two dominated by compression and two by dilation. The boundaries separating these sectors form two perpendicular surfaces referred to as nodal planes (Figure 2) [3].

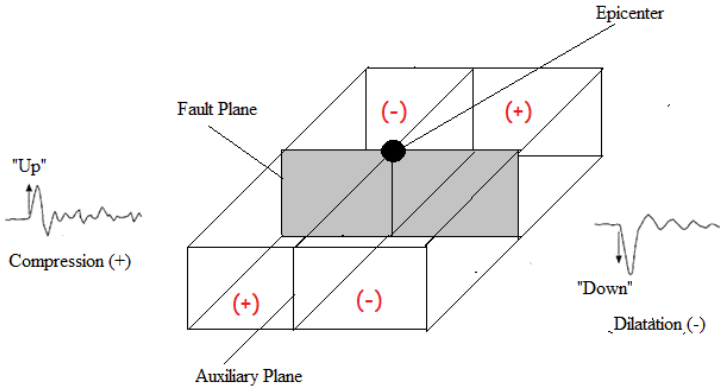

Figure 2: Representation of compression and dilatational first motions of P-waves forming four quadrants separated by nodal planes (Source: [4])

This four-quadrant pattern originates from the physical nature of earthquake slip. Rupture along a fault is equivalent to a double-couple force system produced by shear dislocation within the Earth's crust. The sudden release of stored elastic strain energy generates P-waves that push material in some directions and pull it in others. The distribution of these push–pull directions is what produces the observed pattern of compressional and dilatational first motions, which in turn reveals the possible orientations of the fault. [2]

The two nodal planes obtained from this analysis correspond to the fault plane and an auxiliary plane. Both planes satisfy the first-motion observations, which means that additional geological or seismological evidence is required to identify which one represents the actual slipping surface. [5]

A convenient way to visualize this information is through a focal mechanism diagram, commonly called a beachball. In this representation, shaded and unshaded regions denote compressional and dilatational areas derived from the moment tensor solution. The geometry of these regions defines the strike and dip of the nodal planes, while the rake indicates the direction of movement along the fault surface. Therefore, the beachball serves as a compact visual summary of the earthquake's slip geometry [5].

For the 2015 Gorkha event, the focal mechanism indicates dominant compression in the north–south direction and a gently north-dipping thrust plane, which is consistent with the regional structure of the Main Himalayan Thrust [6].

Because representing orientations directly on a sphere is impractical, the information is transferred to a plane using a stereographic projection. This projection is implemented through a stereonet, which allows three-dimensional orientation data to be displayed on a two-dimensional surface (Figure 3) [2].In this study, the stereonet is constructed using the strike, dip, and rake values obtained from the Global CMT dataset (Table 1) [7].

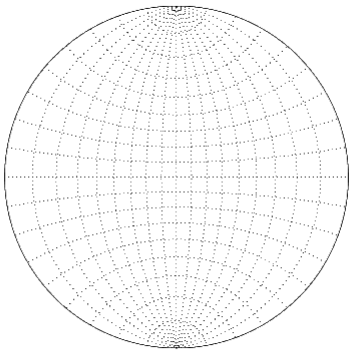

Figure 3: A stereonet used to display a hemisphere on a flat surface (generated using MATLAB)

Plotting these parameters on the stereonet enables visualization of the orientations of the principal stress axes (P, T, and N) and provides a geometric check on the consistency of the focal mechanism solutions prior to generating beachball diagrams. The clustering of P-axes toward the NNE direction confirms the prevailing north–south compressional stress regime responsible for thrust faulting in central Nepal [6].

By integrating first-motion polarity analysis, moment tensor interpretation, stereographic projection, and focal mechanism visualization, a comprehensive geometrical and mathematical understanding of the earthquake source is achieved. This combined methodology forms the basis for determining the fault plane characteristics of the Gorkha earthquake and its associated aftershocks.

2. METHODOLOGY

This study determines the fault plane characteristics of the 2015 Gorkha earthquake and its major aftershocks by integrating moment tensor analysis, stereographic projection, and GIS-based visualization. Two independent seismic catalogs were used to ensure reliability and comparison of focal mechanism solutions.

A. Data Sources

Fault plane parameters and moment tensor solutions were obtained from:

1. Global Centroid Moment Tensor (CMT) catalog developed by Adam Dziewonski and collaborators [7]. This catalog provides six independent moment tensor components along with derived strike, dip, and rake values for global earthquakes.
2. Department of Mines and Geology (DMG), Nepal earthquake catalog [8], which provides focal mechanism parameters computed from regional seismic observations.

Nine significant events (mainshock and aftershocks with Mw ≥ 5) between 25 April

2015 and 16 May 2015 were selected for analysis (Table 1,Table 2 and Table 3)

Table 1: Fault-plane solution parameters of nine earthquakes (1 main shock and 8 after shock) from Central Nepal Himalaya and its adjoining regions.

SN	Date	GMT	Latitude	Longitude	Depth (in Km)	Moment Magnitude (Mw)	Strike Angle (^{0})	Dip Angle (^{0})	Rake Angle (^{0})
1	4/25/2015	6:11:59	27.91	85.33	12	7.9	287	6	96
2	4/25/2015	6:45:53	27.86	84.93	21	6.7	308	23	131
3	4/25/2015	17:42:53	28.06	85.89	20.8	5.3	339	40	-105
4	4/25/2015	23:16:18	27.61	84.96	15	5.1	201	40	-20
5	4/26/2015	7:09:20	27.56	85.95	20.6	6.7	289	14	98
6	4/26/2015	16:26:10	27.56	85.95	19.8	5.2	305	26	115
7	5/12/2015	7:05:27	27.67	86.08	12	7.2	307	11	117
8	5/12/2015	7:37:00	27.37	86.35	20.1	6.1	299	28	116
9	5/16/2015	11:34:13	27.37	86.26	12	5.3	324	34	138

B. Moment Tensor Components and Their Significance

The Global CMT catalog provides six independent components of the seismic moment tensor: mrr, mtt, mpp, mrt, mrp, mtp, defined in a spherical coordinate system where:

- r = radial (upward),
- t = theta (southward),
- p = phi (eastward).

These components form a symmetric moment tensor matrix that represents the double-couple source mechanism of the earthquake. Through eigenvalue decomposition of this matrix, three principal axes are obtained:

- P-axis (maximum compression),
- T-axis (maximum tension),
- N-axis (neutral axis).

From these axes, the strike, dip, and rake of two nodal planes are mathematically derived. These parameters are then used to construct focal mechanism (beachball) diagrams and stereonet plots. Thus, the moment tensor components are the mathematical foundation of the fault plane solution [2], [3] , [7].

Table 2: CMT Harvard Centroid Moment Tensor data where mrr, mtt, mpp, mrt, mrp and mtp are six components of moment Tensor (r for up, t for south and p for east)

SN	Latitude	Longitude	Depth (km)	Moment Magnitude (Mw)	mrr	mtt	mpp	mrt	mrp	mtp
1	27.91	85.33	12	7.9	1.76	-1.82	0.06	8.04	-1.51	0.48
2	27.86	84.93	21	6.7	0.68	-0.74	0.06	0.96	0.19	0.25
3	28.06	85.89	20.8	5.3	-1.04	0.16	0.87	0.16	0.26	-0.17
4	27.61	84.96	15	5.1	-2.08	-2.46	4.54	5.53	-0.9	-1.2
5	27.56	85.95	20.6	6.7	0.6	-0.67	0.07	1.2	-0.23	0.2
6	27.56	85.95	19.8	5.2	5.38	-5.14	-0.24	5.14	-0.18	2.23
7	27.67	86.08	12	7.2	2.7	-2.62	-0.08	8.25	-1.28	1.22
8	27.37	86.35	20.1	6.1	1.37	-1.54	0.17	1.24	0.14	0.43
9	27.37	86.26	12	5.3	0.75	-0.95	0.2	0.83	0.04	0.63

C. Stereonet Construction Using MATLAB

To geometrically validate the focal mechanism solutions, stereographic projection was performed using MATLAB. The strike, dip, and rake values obtained from the Global CMT data (Table 1) were plotted on a stereonet (Figure 3).This allowed visualization of the orientation of nodal planes and clustering of P-axes, confirming the regional north–south compressional stress regime responsible for thrust faulting in central Nepal.

D. Beachball Visualization Using ArcGIS

For spatial visualization of focal mechanisms, the ArcGIS ArcBeachBalls v2.5 toolbox was used. The strike, dip, and rake values from the DMG catalog (Table 3) and Global CMT catalog (Table 1) were input into the toolbox to generate beachball diagrams plotted on the regional map (Figure 4 and Figure 5). This GIS-based approach allows comparison of fault orientations and dip azimuths between the two datasets.

Table 3: Fault-plane solution parameters taken catalogue of the Department of Mines and Geology (DMG), Nepal [8]

ID	Event date (M/D/Y)	Origin time (hr:min:s)	Latitude (N)	Longitude (E)	M w	Depth (in km)	Strike	Dip	Rake	Reference
Main shock										
1	4/25/2015	6:11:24	28.23	84.76	7.8	17	283	52	94	Centroid Source (TWI)
Aftershocks										
2	4/25/2015	6:45:19	28.22	84.9	6.7	20	285	7	86	GFZ
3	4/25/2015	17:42:51	28.35	85.91	5.1	12	264	59	235	Centroid Source (TWI)
4	4/25/2015	23:16:15	27.9	85	5.1	16	302	81	222	Centroid Source (TWI)
5	4/26/2015	7:09:09	27.74	86.06	6.9	16	340	9	137	Centroid Source (TWI)
6	4/26/2015	16:26:07	27.81	85.88	5	14	236	35	62	Centroid Source (TWI)
7	5/12/2015	7:05:18	27.83	86.19	7.3	17	283	8	92	Centroid Source (TWI)
8	5/12/2015	7:17:19	27.86	86.32	5.5	16	250	23	67	Centroid Source (TWI)
9	5/12/2015	7:36:51	27.67	86.39	6.3	15	303	23	123	USGS
10	5/16/2015	11:34:09	27.63	86.26	5.5	10	292	26	106	Centroid Source (TWI)

E. Comparative Analysis

The beachball diagrams obtained from both catalogs were compared to evaluate: Consistency in fault type (thrust, normal, and strike-slip), Orientation of nodal planes, Dip azimuth and rupture direction, and Agreement with the geometry of the Main Himalayan Thrust.

This comparative approach reduces ambiguity and increases confidence in identifying the actual fault plane responsible for the Gorkha earthquake.

3. RESULT AND DISCUSSION

A. Outcome from ArcGIS

From the catalog of the department of mines and geology, beach ball orientation is shown figure below using ArcGIS.

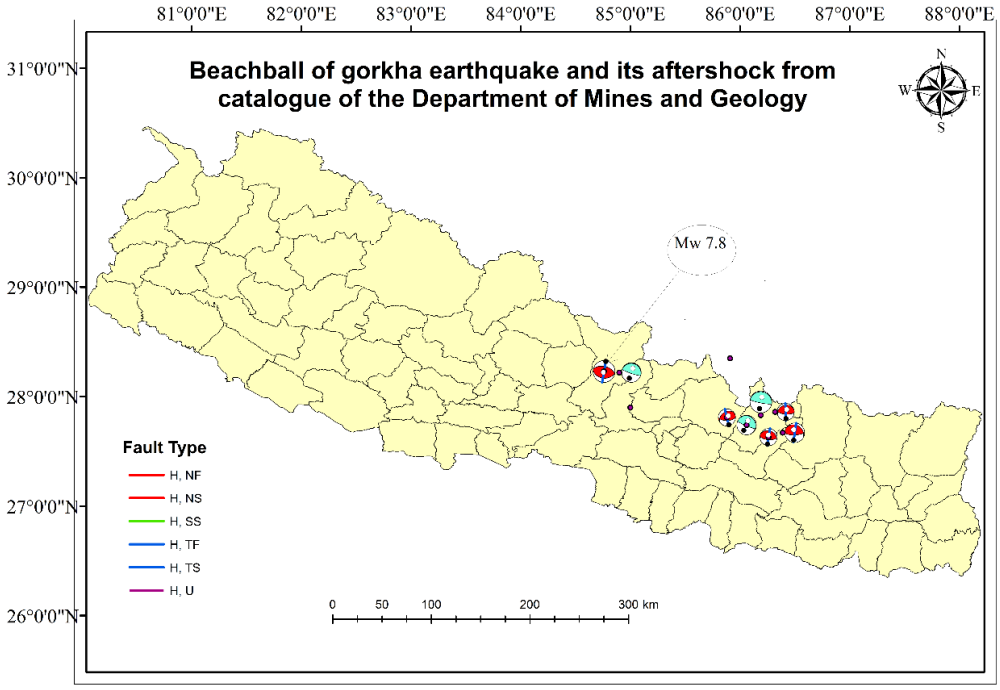

Figure 4: Beachball of Gorkha earthquake and its aftershock from catalogue of the department of mines and geology.

Beachball orientations generated from the Department of Mines and Geology (DMG) catalog using ArcGIS are shown in Figure 4. The focal mechanism of the 25 April 2015 Gorkha earthquake (Mw 7.8) indicates a reverse or thrust faulting mechanism with a shallow north-dipping nodal plane. The compressional quadrants are oriented roughly in the north–south direction, which reflects regional compression caused by the convergence between the Indian and Eurasian plates. The nodal plane orientation suggests slip along a gently dipping thrust interface consistent with the Main Himalayan Thrust.

The aftershock focal mechanisms show similar characteristics to the mainshock. Most events are classified as thrust faulting (TF) with dip azimuth values mainly ranging between about 10° and 190° as shown in Table 4. The distribution of dip azimuth values and the spatial clustering of aftershocks toward the southeast indicate that rupture propagated primarily in that direction. These observations suggest that the earthquake sequence was controlled by the same tectonic structure and dominated by thrust faulting in central Nepal [6].

Table 4: Output (fault type and dip azimuth value) from the ArcGIS beachball toolbox

No	Date	Mw	Dip Azimuth	Fault Type
1	4/25/2015	7.8	10	TF
2			-999	U
3			-999	U
4	4/26/2015	5	166	TF
5			-999	U
6	5/12/2015	5.5	178	TF
7	5/12/2015	6.3	188	TF
8	5/16/2015	5.5	190	TF

*TF- Thrust Fault

Table 5: Output (fault type and dip azimuth value) from the ArcGIS beachball toolbox (global CMT catalog

No	Date	Mw	Dip Azimuth	Fault Type
1	4/25/2015	7.9	-999	U
2	4/25/2015	6.7	187	TF
3	4/25/2015	5.3	351	NF
4	4/25/2015	5.1	-999	U
5	4/26/2015	6.7	192	TF
6	4/26/2015	5.2	196	TF
7	5/12/2015	7.2	194	TF
8	5/12/2015	6.1	190	TF
9	5/16/2015	5.3	200	TF

*TF- Thrust Fault
*NF- Normal Fault

B. Outcome from MATLAB

For data source of the global CMT catalog,

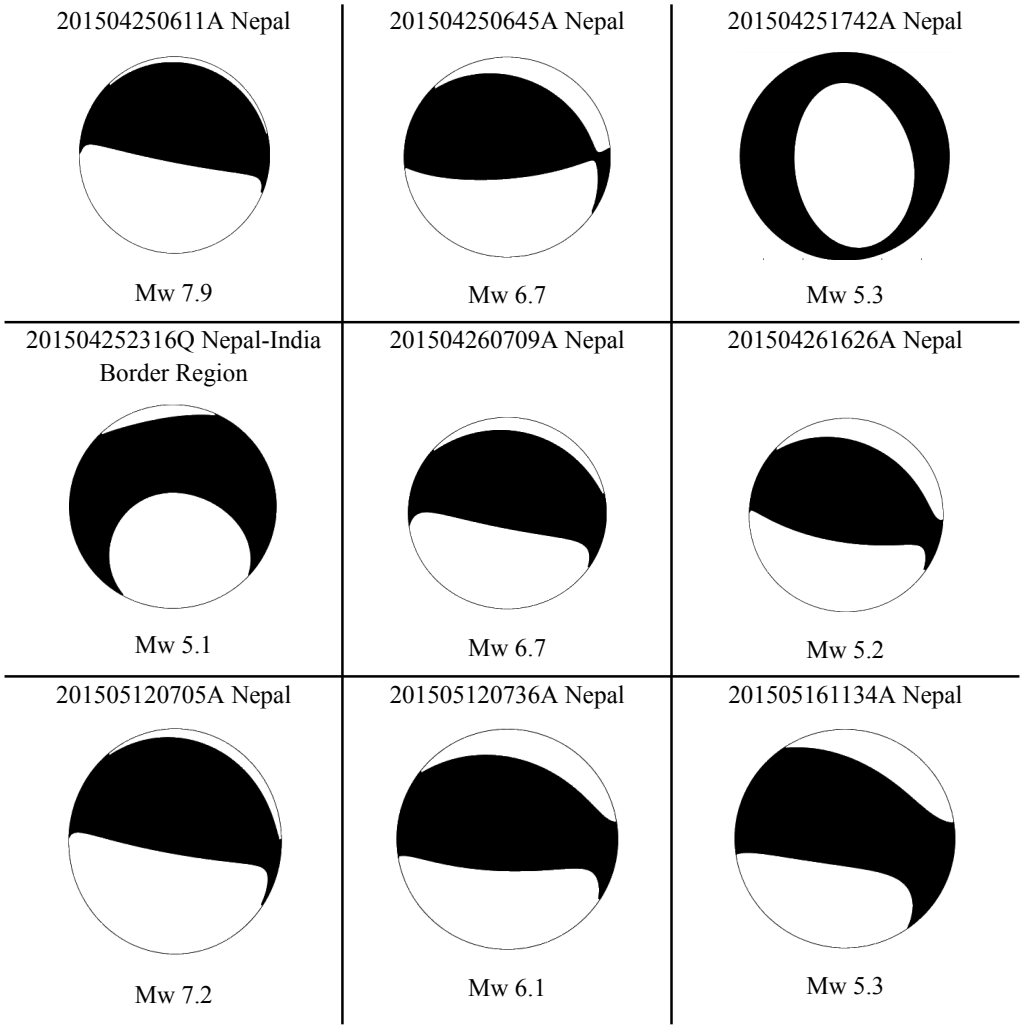

Figure 5: Beachball of Gorkha earthquake and its aftershock from a source of global CMT catalog using MATLAB.

Beachball diagrams generated using Global CMT data in MATLAB are presented in Figure 5. The focal mechanism of the mainshock also indicates reverse faulting with shallow northward dip and approximately east–west strike. Most of the aftershocks show similar focal mechanisms, confirming compressional tectonics across the Himalayan region.

Comparison between Figure 4 and Figure 5 shows good agreement between the DMG catalog and Global CMT results. Both datasets indicate dominant thrust faulting, shallow north-dipping nodal planes, and similar strike directions. A few events show minor variations such as normal fault components, which may be related to local stress redistribution after the mainshock [9].

C. Fault Plane Ambiguity

Each focal mechanism solution provides two possible nodal planes. For the Gorkha earthquake, the shallow north-dipping plane agrees with the regional geometry of the Main Himalayan Thrust and the southeastward aftershock distribution. Therefore, this plane is interpreted as the actual fault plane, while the opposite steeply dipping plane is considered the auxiliary plane [9], [6].

D. Rupture Propagation Characteristics

The concentration of aftershocks toward the southeast suggests unilateral rupture propagation from the hypocenter. The shallow thrust geometry and compressional axis orientation support this interpretation. The lack of clear surface rupture indicates that slip remained at depth along the Main Himalayan Thrust, which is typical for Himalayan megathrust earthquakes [2].

The combined ArcGIS and MATLAB analysis indicates that the 2015 Gorkha earthquake was dominated by shallow north-dipping thrust faulting. The similarity between mainshock and aftershock mechanisms suggests rupture along a common fault segment. These findings are consistent with the regional tectonic setting and provide useful information for understanding seismic hazard in central Nepal.

4. CONCLUSION

The focal mechanism analysis of the 2015 Gorkha earthquake and its aftershocks indicates a dominant reverse faulting mechanism with a shallow north-dipping nodal plane. The beachball diagrams obtained from both DMG and Global CMT datasets show similar strike, dip, and compression directions, confirming that the earthquake sequence was controlled by a common thrust fault system associated with the Main Himalayan Thrust.

The spatial distribution of aftershocks suggests that rupture propagated mainly toward the southeast from the hypocenter. The similarity between the mainshock and aftershock mechanisms indicates that the events occurred along the same gently dipping fault plane. The absence of surface rupture further implies that slip remained confined to deeper portions of the fault.

Overall, the results confirm that the 2015 Gorkha earthquake was governed by shallow thrust faulting related to regional plate convergence. The consistency between the two datasets increases confidence in the interpreted fault geometry and provides useful information for understanding seismic hazard in central Nepal.

ACKNOWLEDGMENTS

The author would like to express sincere gratitude to the Department of Mines and Geology (DMG), Nepal, and the Global Centroid Moment Tensor (CMT) catalog for

providing earthquake data used in this study. The author is also thankful to all researchers whose published works helped in understanding the tectonic setting of the 2015 Gorkha earthquake.

Special thanks are extended to teachers and colleagues for their guidance and support during the preparation of this research. Finally, the author acknowledges all individuals who directly or indirectly contributed to the completion of this work.

REFERENCES

[1] H. P. R.K. Tiwari, "Geodynamics of Gorkha earthquake (Mw 7.9) and its aftershocks," The Himalayan Physics, pp. 103-109, 2020.

[2] M. W. Seth Stein, An Introduction to Seismology, Earthquakes, and Earth Structure, UK: Blackwell Publishing, 2003.

[3] A. jj and R. yy, Quantitative Seismology., University Science Books, 2002.

[4] M. Ivancic, Z. Mihajlovic and I. Ivancic, "Seismic data visualisation," 2015.

[5] USGS, "United States Geological Survey (USGS)," 2015. [Online]. Available: https://earthquake.usgs.gov/earthquakes/eventpage/us20002926/executive. [Accessed 28 04 2022].

[6] R. Grandin, M. Vallée, C. Satriano, R. Lacassin, Y. Klinger, M. Simoes and L. Bollinger, "Rupture process of the Mw = 7.9 2015 Gorkha earthquake (Nepal): Insights into Himalayan megathrust segmentation," Geophysical Research Letters, vol. 42, no. 20, pp. 8373-8382, 10 2015.

[7] A. M. Dziewonski, G. Ekström, J. E. Franzen and J. H. Woodhouse, "Global seismicity of 1981: centroid-moment tensor solutions for 542 earthquakes," Physics of the Earth and Planetary Interiors, vol. 50, no. 2, pp. 155-182, 1988.

[8] L. Adhikari, U. Gautam, B. Koirala, M. Bhattarai, T. Kandel, R. Gupta, C. Timsina, N. Maharjan, K. Maharjan, T. Dahal, R. Hoste-Colomer, Y. Cano, M. Dandine, A. Guilhem Trilla, S. Merrer, P. Roudil and L. Bollinger, "The aftershock sequence of the 2015 April 25 Gorkha–Nepal earthquake," Geophysical Journal International, vol. 203, pp. 2119-2124, 4 2015.

[9] W. Fan and P. M. Shearer, "Detailed rupture imaging of the 25 April 2015 Nepal earthquake using teleseismic P waves," Geophysical Research Letters, vol. 42, no. 14, pp. 5744-5752, 7 2015.

[10] J. A. Conder, "Open SIUC," 17 04 2017. [Online]. Available: https://opensiuc.lib.siu.edu/geol_comp/5/. [Accessed 20 04 2022].

[11] R. K. Tiwari and H. P. Paudyal, "Geodynamics of Gorkha earthquake (Mw 7.9) and its aftershocks," Himalayan Physics, pp. 103-109, 12 2020.

[12] L. Zhang, J. Li, W. Liao and Q. Wang, "Source rupture process of the 2015 Gorkha, Nepal Mw7.9 earthquake and its tectonic implications," Geodesy and Geodynamics, vol. 7, no. 2, pp. 124-131, 3 2016.

[13] J. Galetzka, D. Melgar, J. F. Genrich, J. Geng, S. Owen, E. O. Lindsey, X. Xu, Y. Bock, J.-P. Avouac, L. B. Adhikari, B. N. Upreti, B. Pratt-Sitaula, T. N. Bhattarai, B. P. Sitaula, A. Moore, K. W. Hudnut, W. Szeliga, J. Normandeau, M. Fend, M. Flouzat, L. Bollinger, P. Shrestha, B. Koirala, U. Gautam, M. Bhatterai, R. Gupta, T. Kandel, C. Timsina, S. N. Sapkota, S. Rajaure and N. Maharjan, "Slip pulse and resonance of the Kathmandu basin during the 2015 Gorkha earthquake, Nepal," Science, vol. 349, no. 6252, pp. 1091-1095, 9 2015.